Supplementary Information

Direct Photoactivation of a Nickel-Based, Water-Reduction Photocathode by a Highly Conjugated Supramolecular Chromophore

Bing Shan,[†] Animesh Nayak,[†] Renato N. Sampaio, Michael S. Eberhart, Ludovic Troian-Gautier, M. Kyle Brennaman, Gerald J. Meyer and Thomas J. Meyer*

Department of Chemistry, University of North Carolina at Chapel Hill, Chapel Hill, NC 27599-3290, United States

† These authors contributed equally to this work.

*Corresponding author.

Table of Contents

Figure S1. Simplified scheme for the synthetic procedure of ZnPRu^{2+}.
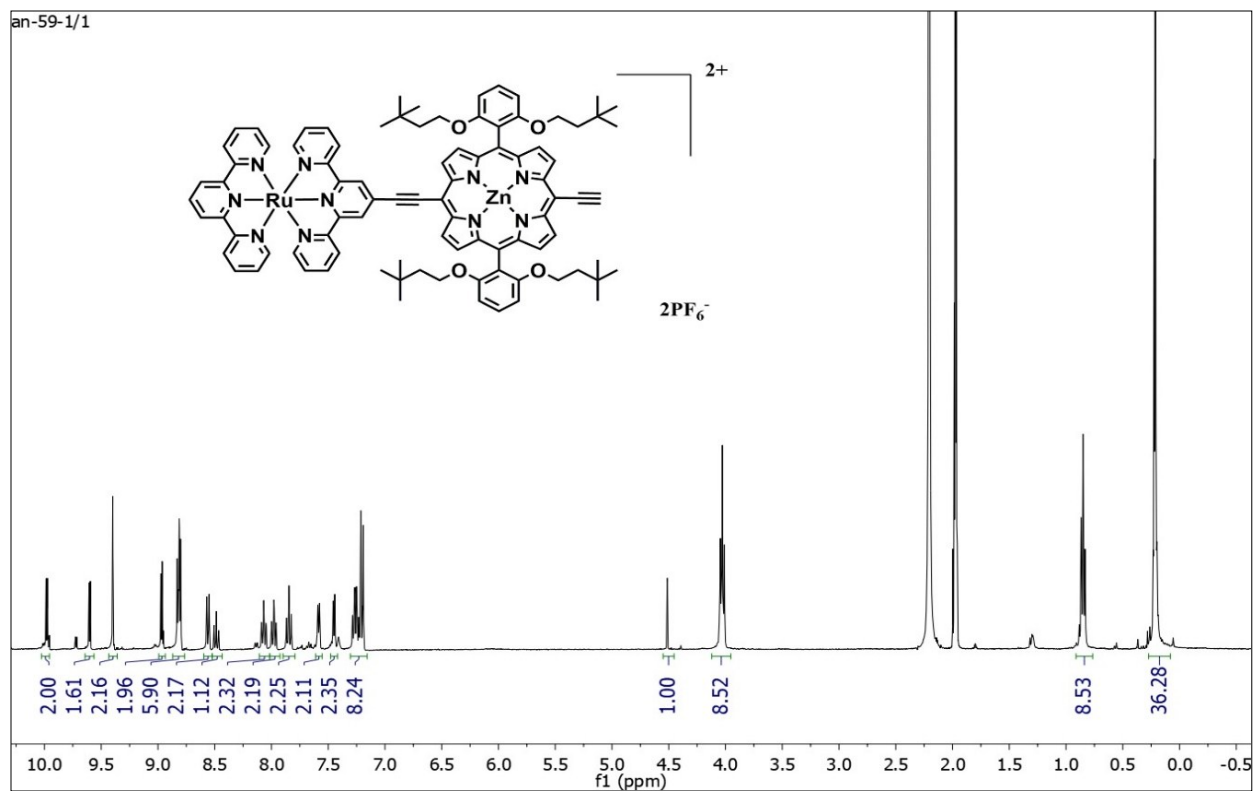
Figure S2. ^{1}H NMR (400 MHz) of RuPZnE in CD$_3$CN.
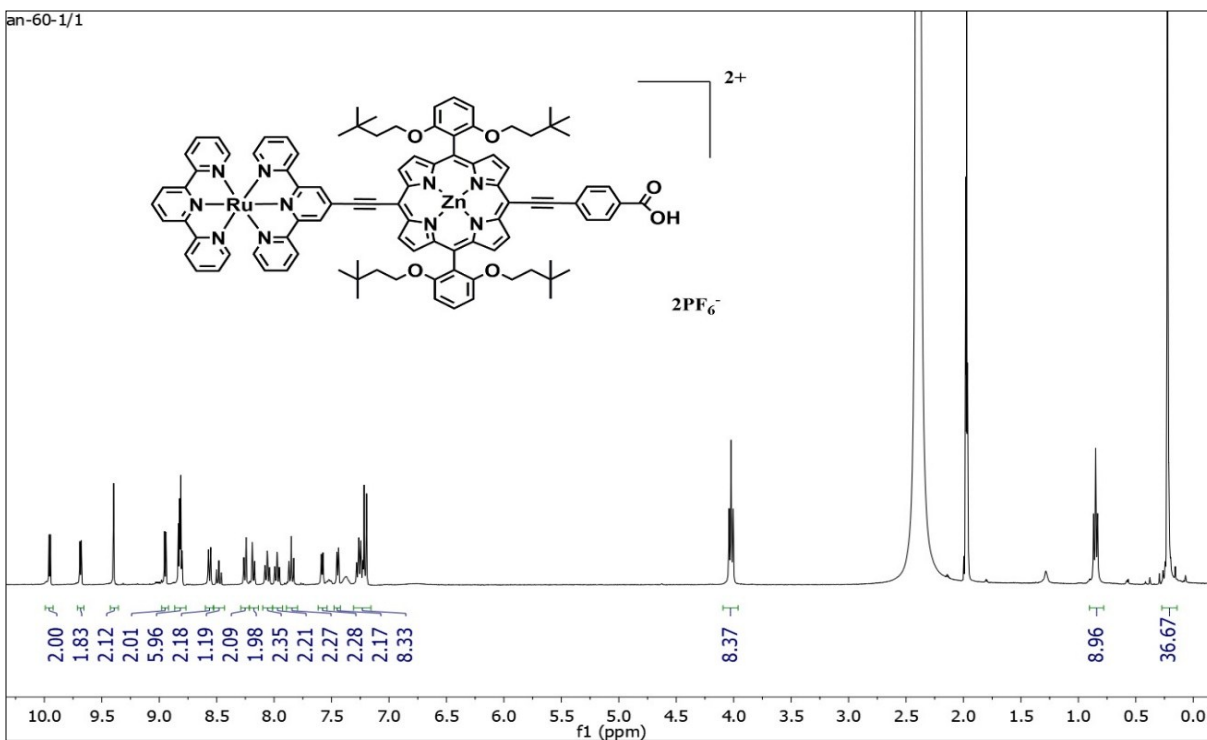
Figure S3. ^{1}H NMR (400 MHz) of ZnPRu^{2+} in CD$_3$CN.
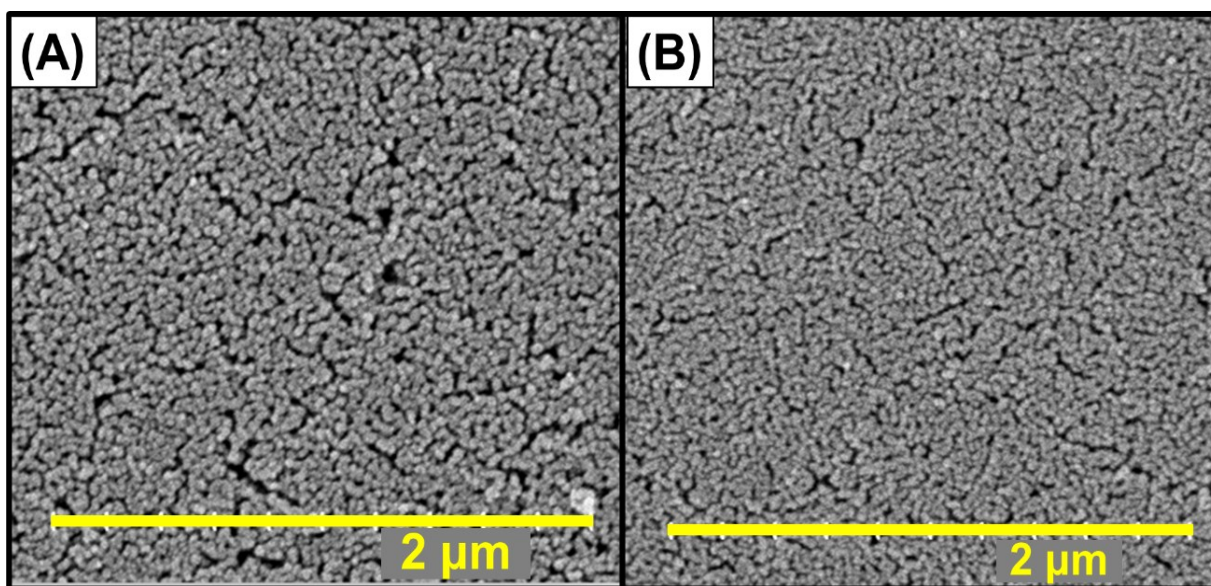
Figure S4. Surface SEM of the photocathodes NiO|-ZnPRu^{2+}|NiMo$_{0.05}$S$_x$ (A) and NiO|-ZnPRu^{2+} (B).
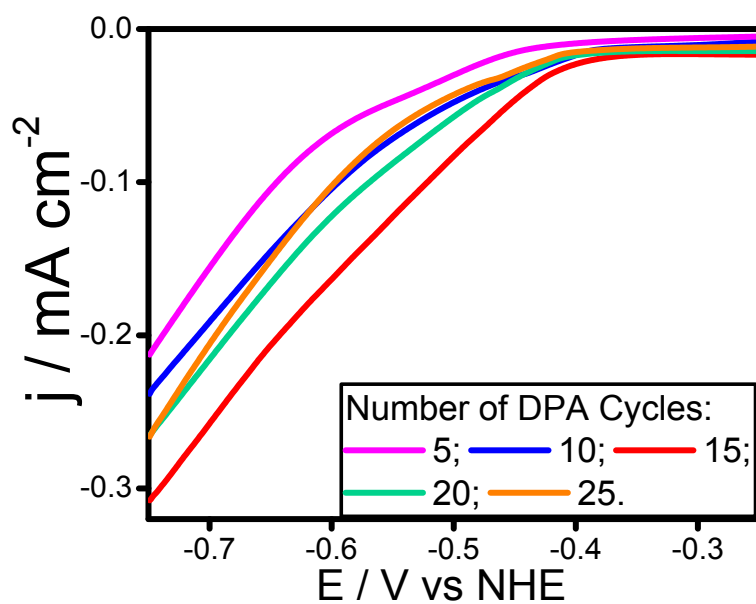
Figure S5. Linear sweep voltammograms of NiO|-ZnPRu^{2+}|NiMo$_{0.05}$S$_x$ with the catalyst from various DPA cycles in pH 4.5 acetate buffer.
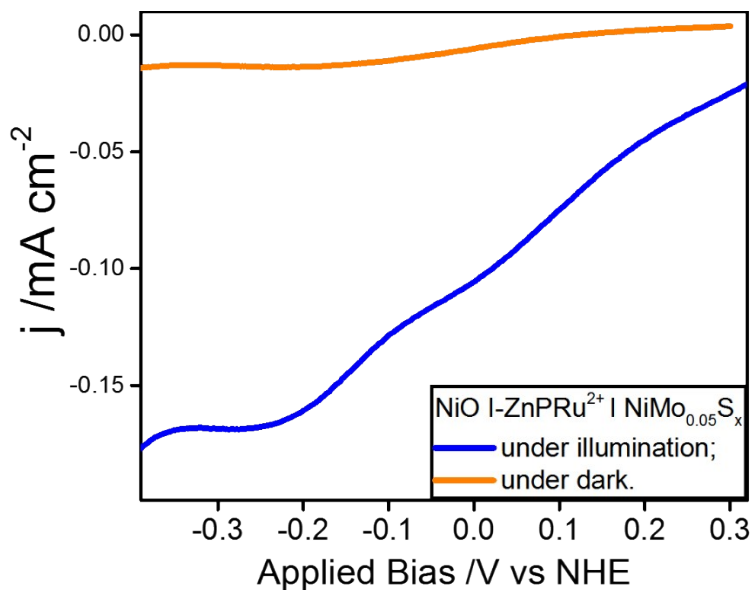
Figure S6. Linear sweep voltammograms for NiO|-ZnPRu^{2+}|NiMo$_{0.05}$S$_x$ under dark (orange trace) or illumination (10 mW/cm^2 blue LED) (blue trace) in pH 4.5 acetate buffer. Scan rate: 5 mV/s.
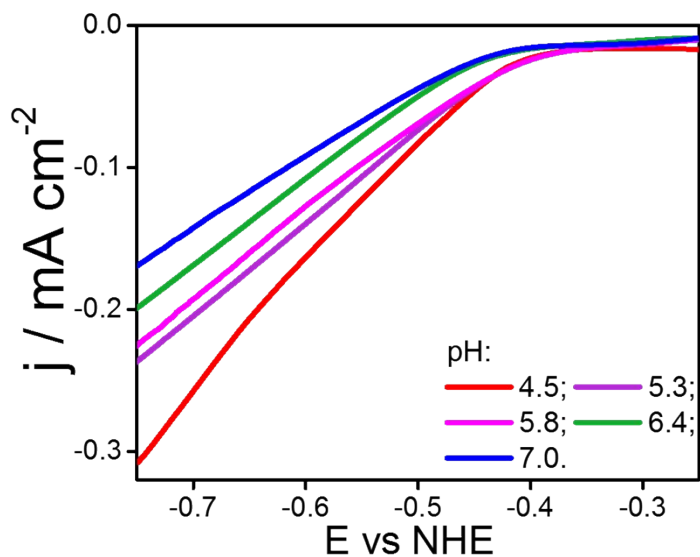
Figure S7. Linear sweep voltammograms of NiO|-ZnPRu^{2+}|NiMo$_{0.05}$S$_x$ with the catalyst from 15-cycle DPA in pH 4.5-7.0 buffers.
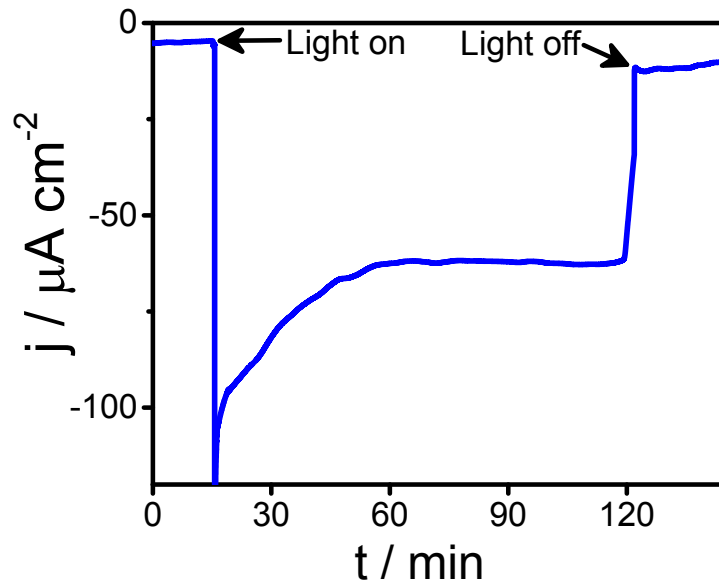
Figure S8. Photocurrents (j/μA cm^{-2}) showing long-term photoelectrocatalysis by the photocathode NiO|-ZnPRu^{2+}|NiMo$_{0.05}$S$_x$ with catalyst form 15-cycle DPA and in pH 4.5 acetate buffer with an applied bias of -0.05 V vs NHE.
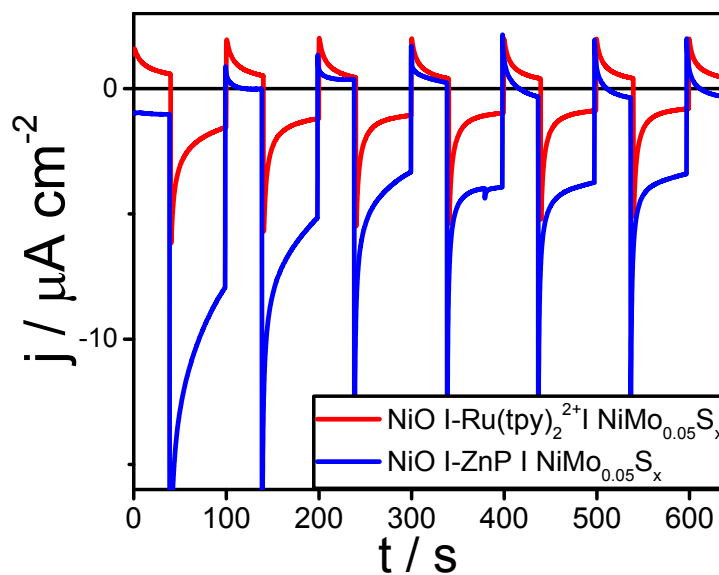
Figure S9. Photocurrents for NiO|-Ru(tpy)$_2^{2+}$|NiMo$_{0.05}$S$_x$ (red curve) and NiO|-ZnP|NiMo$_{0.05}$S$_x$ (blue curve) in pH 4.5 acetate buffer with an applied bias of -0.05 V vs NHE.
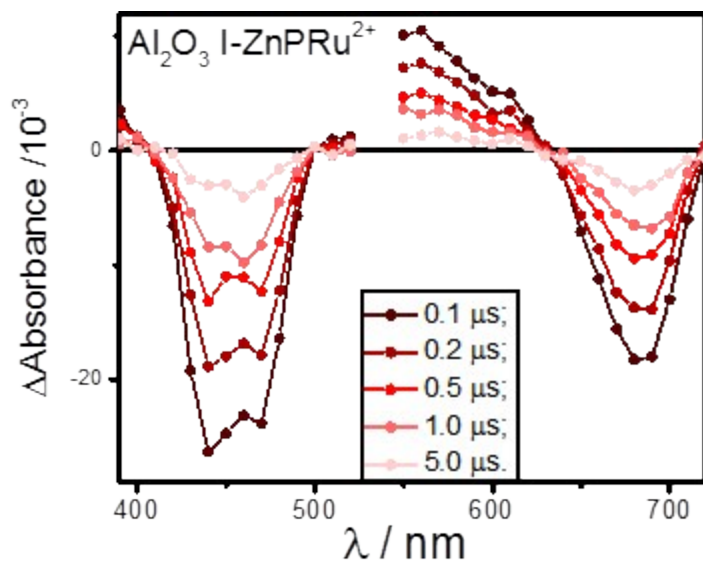
Figure S10. Nanosecond transient absorption (*ns*TA) following excitation of $Al_2O_3|–ZnPRu^{2+}$ at 532 nm as a function of time delay after the laser pulses. Solution medium: N_2 degassed pH 4.5 acetate buffer.
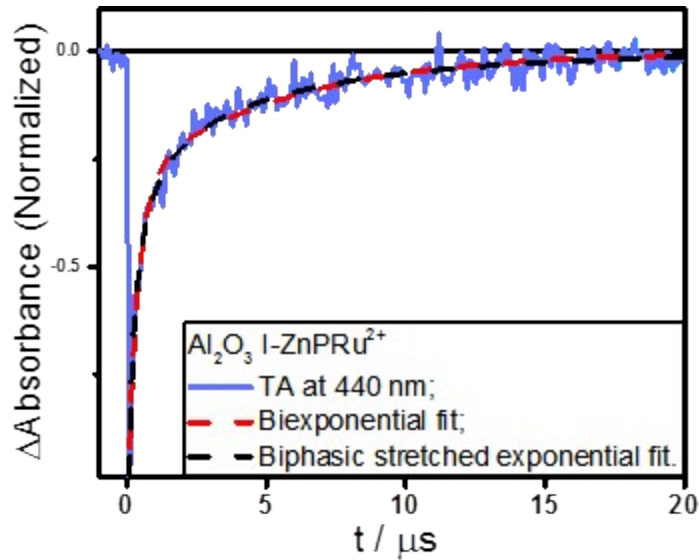
Figure S11. Time-resolved *ns*TA at 440 nm following excitation of $Al_2O_3|–ZnPRu^{2+}$ at 532 nm (blue, solid), biexponential fit (red, dashed) and biphasic stretched exponential fit (black, dashed). Solution medium: N_2 degassed pH 4.5 acetate buffer (aq., 0.1 M).
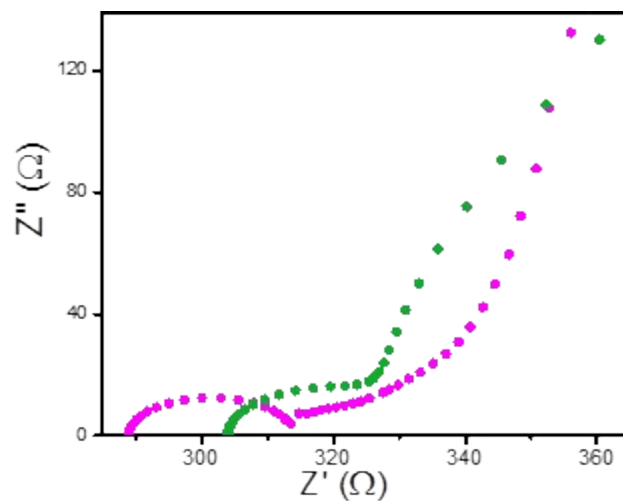
Figure S12. Nyquist plots for a photocathode NiO|-ZnPRu^{2+}|NiMo$_{0.05}$S$_x$ after immersion in pH 4.5 buffer for 3 hours in the dark (pink) and a photocathode NiO|-ZnPRu^{2+}|NiMo$_{0.05}$S$_x$ after 3-hour PEC (green). Comparison of the Nyquist plots indicates that proton intercalation is not a main cause for the increased resistance in charge transfer and contact surface of the "degraded" photocathode.

Faradaic Efficiency and Quantum Yield of Hydrogen Calculation.

The Faradaic efficiency was determined by the equation, Faradaic efficiency = $\dfrac{mols\ of\ H_2 \times 2}{moles\ of\ electrons}$. Based on the photocurrent results in Figure S6 and the quantification of hydrogen evolution from Gas Chromatography measurements, the Faradaic efficiency was determined to be 78.5±2.4% over 2-hour period of photoelectrocatalysis.

The quantum yield of hydrogen was determined to be 1.29±0.04%, according to the equation,

$$\eta_{QY} = \frac{n(H_2) \times N_A \times h \times c \times 2}{\lambda \times t \times I \times A}$$

, with n(H$_2$): moles of H$_2$ (moles), N$_A$: Avogadro constant (6.02×10^{23} mol^{-1}), h: Planck constant (6.63×10^{-34} kg m^2 s^{-1}), c: speed of light (3.0×10^8 m s^{-1}), λ: wavelength (4.45×10^{-7} m), t: irradiation time (s), I: light intensity (0.01 W m^{-2}) and A: irradiated area (1.0 m^2).